Journal of Materials Chemistry A

Accepted Manuscript

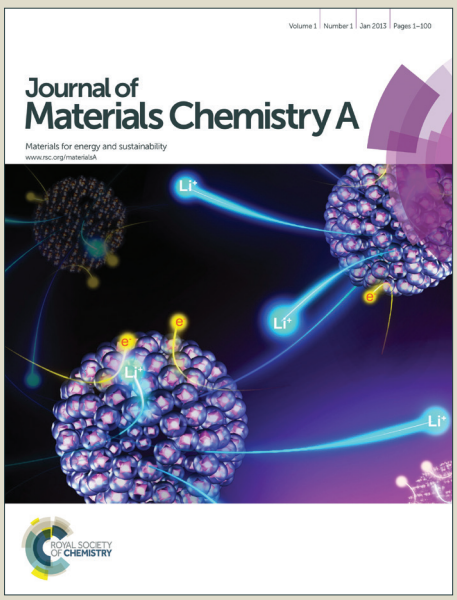

ROYAL SOCIETY OF CHEMISTRY

www.rsc.org/materialsA

Cite this: DOI: 10.1039/c0xx00000x

www.rsc.org/xxxxxx

ARTICLE TYPE

Room Temperature Interfacial Reaction-Directed Synthesis of Hierarchically Porous Ceria from a Water-Soluble Precursor

Guozhu Chen,*[a] Qihui Xu,[a] Yong Wang,[a] Guolong Song [a] and Weiliu Fan [b]

Received (in XXX, XXX) Xth XXXXXXXXX 20XX, Accepted Xth XXXXXXXXX 20XX

DOI: 10.1039/b000000x

Unlike the conventional calcination of cerium precursors at elevated temperature, hierarchically porous ceria was successfully synthesized via an interfacial reaction between water-soluble cerium sulfate ($Ce_2(SO_4)_3$) precursor and NaOH in ethanol at room temperature. Neither additional surfactant molecules nor calcination was employed during the whole preparation process. It was found that the as-prepared ceria inherited well the shape and dimensions of the hierarchically flowerlike $Ce_2(SO_4)_3$ precursor after interfacial reaction. The concentration of sulfuric acid was demonstrated to play a great role in controlling the precursor's morphology. Compared with ceria derived from direct calcination of the same $Ce_2(SO_4)_3$ precursor, the one obtained from interfacial reaction was far more reactive in CO oxidation due to its well-kept hierarchically porous morphology and high surface area. This work is expected to open a new, simple avenue for the synthesis of hollow nanomaterials from water-soluble precursors.

Introduction

Ceria, as a key component in the formulation of catalysts and catalyst supports, has received extensive investigations on various catalytic reactions owing to its excellent redox property and high oxygen storage capacity.[1-5] It is well demonstrated that the catalytic performance of ceria is largely dependent on its morphology and structure.[6-13] Thus, porous ceria has shown great potential as a versatile catalyst and a catalyst support because this kind of structure with large surface area not only favors transportation of reactant molecules to the active sites of ceria more effectively, but also facilitates dispersion of noble metal nanoparticles (NPs) when ceria is engaged as a support.[14-19] To aim at synthesizing porous materials, one general way is the utilization of porous templates to construct the desired structures. For example, mesoporous ceria was prepared from the nanocasting pathway with SBA-15 and KIT-6 as templates, which were filled with cerium precursors to be cast, followed by the removal of initial templates.[14, 15] Despite its elegance and generality in synthesis of mesoporous materials, there are still remaining challenges in the nanocasting strategy: the requirement of relatively large numbers of steps, the compatibility of target material with the conditions of the template-removal process, and stringent controls in precursor concentration. In addition, this method has a certain degree of difficulty in controlling diverse morphologies, such as hierarchically porous hollow structure.

Thanks to the assistance of polymers/surfactants, cerium-containing precursors with various morphologies have been successfully synthesized. After calcination treatment, these precursors can be transformed into ceria keeping their morphologies.[20-26] For example, Wan *et al.* fabricated flowerlike ceria through a cerium alkoxide precursor that was prepared in the presence of tetrabutylammonium bromide and ethylene glycol, followed by a calcination step at 450 °C.[20] Sun *et al.* also synthesized flowerlike mesoporous ceria via calcination of flowerlike $Ce(OH)CO_3$, which was obtained by a simultaneous polymerization-precipitate reaction, metamorphic reconstruction, and mineralization under hydrothermal condition.[21] In addition, self-assembled hierarchical $Ce(SO_4)_2$ microdiscs were first synthesized and their conversion into ceria microdiscs were achieved at 1100 °C for 4 h.[22] Recently a flowerlike morphology of cerium oxalate precursor could be synthesized in the presence of poly(vinyl-pyrrolidone) and H_2O_2 under hydrothermal conditions. Upon calcination, the cerium oxalate precursor transformed into ceria with initial flowerlike morphology.[23] By controlling the aggregation behavior of mixtures of the alkaline amino acid l-arginine (l-Arg) and bis(2-ethylhexyl)phosphoric acid in water, Hao *et al.* prepared porous ceria by calcination of the so-called sponge phase template containing cerium salt.[24] Although the calcination is an efficient way for fabricating desired structured ceria by the decomposition of cerium-containing precursors, disadvantages of a complicated process of precursor preparation, rigorous calcination step required for the removal of engaged polymers/surfactants as well as for the transformation into ceria, would inevitably raise environmental pollution and energy consumption. More importantly, for those precursors that may possess promising morphologies but are difficult to decompose into metal oxide, *e.g.* sulfates in comparison to corresponding carbonates or nitrates, the major problem is the structure collapse during the transformation at high temperature. Therefore, both the search of novel precursors and mild transformation conditions are areas of interest not only for ceria derived from cerium-containing precursors, but also for the construction of other metal oxides.

Solid-liquid interfacial reaction-based sacrificial template approaches are recognised as a good strategy to synthesize hollow and/or mesoporous materials, because the employed templates participate in interfacial chemical reaction, thus the calcination step is avoided.[27-30] For example, hollow ZnO architecture can be fabricated by mixing $Zn_5(CO_3)_2(OH)_6$ microspheres with KOH aqueous solution at room temperature without calcination.[27] After mixing $MnCO_3$ with $KMnO_4$ aqueous solution for a certain time, hollow MnO_2 was achieved after acid-washing residual $MnCO_3$ sacrificial template.[28] Recently we chose $Ce(OH)CO_3$ nanorods as templates to react with NaOH and $KMnO_4$ aqueous solution respectively, hollow ceria and Ce-Mn bimetal oxide nanotubes were obtained when the unreacted $Ce(OH)CO_3$ was removed by acid.[29, 30] In these interfacial reactions, the engaged precursors are all insoluble in water. If the precursor is water-soluble, the residual precursor can be removed by water instead of acid or other post-treatment. However, exploration of water-soluble precursors in the synthesis of hollow mesoporous structured materials has been rarely reported so far.

In this paper, we report a simple and robust approach for the synthesis of hollow mesoporous ceria by choosing $Ce_2(SO_4)_3$, a water-soluble compound but insoluble in ethanol, as a precursor to conduct a solid-liquid interfacial reaction with NaOH in ethanol. After mild reaction at room temperature, the $Ce_2(SO_4)_3$ successfully converts into ceria without calcination or acid/base etching process. The obtained ceria not only inherits initial hollow hierarchical morphology of $Ce_2(SO_4)_3$ precursor but also possesses mesoporous structure. Due to its high surface area, the hollow mesoporous ceria exhibits high catalytic activity toward CO oxidation in comparison to the ceria derived from the direct calcination of $Ce_2(SO_4)_3$.

Experimental Section

Materials:

Cerium(III) chloride heptahydrate ($CeCl_3 \cdot 7H_2O$), sodium hydroxide (NaOH), concentrated sulfuric acid (H_2SO_4) and ethanol were purchased from Sinopharm Chemical Reagent Co. Ltd. They were of analytical grade and were used without further purification.

Synthesis of $Ce_2(SO_4)_3$ precursor

$Ce_2(SO_4)_3$ can be easily prepared by mixing cerium(III) chloride and concentrated sulfuric acid. In a typical synthesis, 148 mg of $CeCl_3 \cdot 7H_2O$ was firstly dissolved in 15.8 ml of anhydrous ethanol under vigorous magnetic stirring, 0.2 mL of H_2SO_4 (5M) was then added into the ethanol solution. The obtained white slurry was transferred into a Teflon-lined steel autoclave and heated for 3 h at 160 ^oC in an electric oven. After the autoclave was cooled to room temperature, white products were collected and washed with ethanol for 3 times and dried overnight at 80^oC.

Synthesis of Ceria

150 mg of prepared $Ce_2(SO_4)_3$ was dispersed in 30 mL of saturated NaOH ethanol solution at room temperature, and kept still for 4 days. Finally, the sample was thoroughly washed with ultrapure water and dried at 80 °C.

Synthesis of Ceria/Au

Deposition-precipitation method was employed to prepare ceria/Au composites. The pH of $HAuCl_4 \cdot 3H_2O$ solution (1 g/100 mL) was adjusted to ~9.0 using $(NH_4)_2CO_3$ solution, and the resulting solution was heated to 60 °C. Then the ceria was added, and the slurry was magnetically stirred for 3 h. The nominal Au loading was 3 wt%. The solids were centrifuged and washed three times with distilled water, dried and calcined at 300 ^oC for 3 h.

Ceria was also achieved by direct calcination of $Ce_2(SO_4)_3$ at ~850 ^oC for 2 h (denoted as C-ceria) to compare with ceria prepared from interfacial reaction between $Ce_2(SO_4)_3$ and NaOH (denoted as I-ceria).

Characterization

The as-prepared samples were characterized by X-ray powder diffraction (XRD) on a Japan Rigaku D/Max-γA rotating anode X-ray diffractometer equipped with Cu Kα radiation (λ=1.54178 Å) in the 2θ range from 20 to 80^o. The morphology and structure of samples were studied by field emission scanning electron microscopy (FE-SEM) (JSM-6700F), transmission electron microscopy (TEM) (JEOL 6300, 100 kV), and X-ray photoelectron spectrometer (XPS) with Al Kα radiation. The Au contents in ceria/Au samples were determined by inductively coupled plasma mass spectrometer (ICP-MS, Thermo Scientific XSeries-2).

N_2 adsorption-desorption isotherms were measured at 77 K on a Micromeritics ASAP 2020 surface area & pore size analyzer. Before measurement, all samples were outgassed in vacuum at 300 ^oC for 3 h. The Brunauer-Emmett-Teller (BET) method was used to calculate the surface areas of samples. The pore size distributions were derived from the desorption branches of the isotherms using the Barrett-Joyner-Halanda (BJH) method.

Hydrogen temperature-programmed reductions (H_2-TPR) of the samples were carried out in a conventional flow system equipped with a thermal conductivity detector. A 50 mg of sample was used and pretreated in a 5% O_2/N_2 flow (40 mL·min^{-1}) at 400 ^oC for 30 min prior to run. After the sample was cooled to room temperature, a 10% H_2/N_2 mixture gas (40 mL min^{-1}) was introduced and the reactor was heated at a rate of 10 $^oC \cdot min^{-1}$ from room temperature to ~800 ^oC.

Catalytic activity was measured using a continuous flow fixed-bed micro-reactor at atmospheric pressure. In a typical experiment, the system was first purged with high purity N_2 gas and then a gas mixture of $CO/O_2/N_2$ (1:10:89) was introduced into the reactor which contained 50 mg samples at a flow rate of 50 mL·min^{-1}, corresponding to a space velocity of 60,000 mL·h^{-1}·g^{-1} of catalyst. Gas samples were analyzed with an online infrared gas analyzer (Gasboard-3100, China Wuhan Cubic Co.).

Results and Discussion

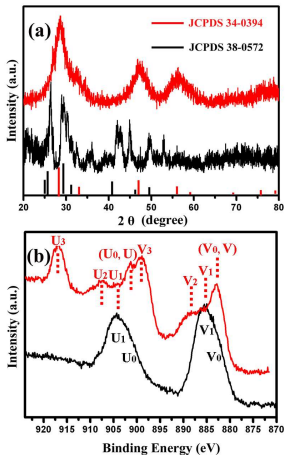

Fig. 1 (a) XRD patterns and (b) Ce 3d XPS spectra of $Ce_2(SO_4)_3$ precursor (black line) and transformed I-ceria (red line).

It should be noted that $Ce_2(SO_4)_3$ easily dissolves in water but precipitates in ethanol, as reported in our previous work.[31] Therefore restriction of water content in solvent during the preparation process and avoidance of water washing in the $Ce_2(SO_4)_3$ precursor purification step are both important and necessary.

The phase purity and crystal structure of the obtained samples were examined by XRD. Fig. 1 shows that the precursor mainly exists as orthorhombic $Ce_2(SO_4)_3 \cdot nH_2O$ (JCPDS file no. 38-0572), other phases with different hydrate number cannot be completely excluded since $Ce_2(SO_4)_3$ displays great diversity in the hydrate number.[32] After interfacial reaction, the diffraction pattern of the sample can be indexed as a face-centered cubic pure phase of ceria without any residual precursor (JCPDS no.34-0394). It is reasonable that the residual $Ce_2(SO_4)_3$ precursor, if any, could be removed by water during the washing step. The average crystallite size of the as-prepared ceria calculated from (220) reflection broadening is around 3 nm. XPS was also used to examine the valence states of Ce 3d during the transformation, as shown in Fig 1b. Two obvious peaks, U_1 and V_1, and two minor peaks, U_0 and V_0, characteristic of Ce(III), are present in the precursor, while peaks labeled U, U_2, U_3, V, V_2, and V_3, characteristic of Ce(IV), are observed in the ceria, indicating the Ce(III) transforms into Ce(IV) after the interfacial reaction.[20]

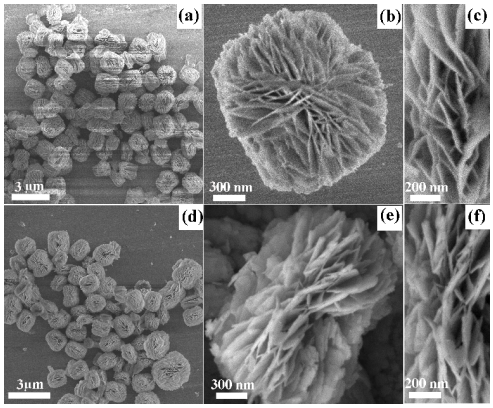

Fig. 2 SEM images of $Ce_2(SO_4)_3$ precursor (a-c) and transformed I-ceria (d-f) with different magnification.

The size and morphology of the products were examined by FE-SEM and TEM measurements. Fig. 2a shows that as-synthesized $Ce_2(SO_4)_3$ precursor is nearly mono-disperse with hierarchically flowerlike texture. The magnified SEM images in Fig. 2b, c clearly show that the flowerlike particle is actually composed of many nanosheets as the petals with an average thickness of about 20-30 nm. These nanosheets interweave, resulting in an open porous structure. After interfacial reaction between $Ce_2(SO_4)_3$ and NaOH, I-ceria particles largely inherit the shape and dimensions of the $Ce_2(SO_4)_3$ precursor (Fig. 2d), except are less smooth on the edge of nanosheets (Fig. 2e, f).

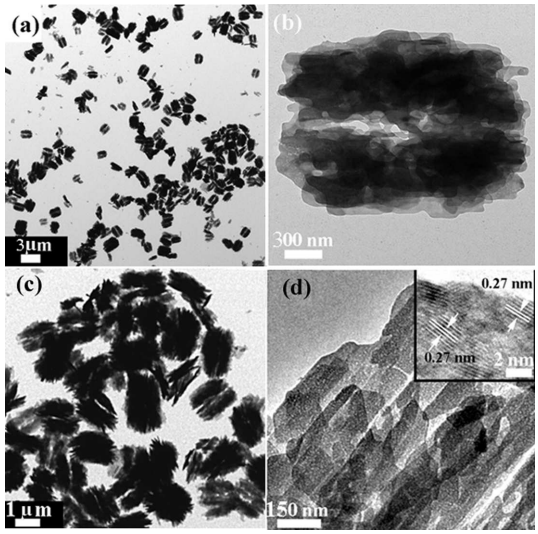

Fig. 3 TEM images of $Ce_2(SO_4)_3$ precursor (a, b) and transformed I-ceria (c, d) with different magnification. Inset in (d) is the high-resolution TEM image of I-ceria.

Fig. 3 displays the TEM images of $Ce_2(SO_4)_3$ precursor and its transformed I-ceria under different magnification. As shown in Fig. 3a, b, the $Ce_2(SO_4)_3$ precursor holds square-like profile with jagged worm-like edge. Furthermore, most particles exhibit hollow structure, reflecting from the sharp contrast between the edge and centre parts in Fig. 3b. Unfortunately, it is hard to acquire a clean image under higher magnification, due to the existence of crystal water in $Ce_2(SO_4)_3$ precursor (Fig. S1). However, the transformed I-ceria not only inherits well the hierarchically hollow structure of $Ce_2(SO_4)_3$ precursor (Fig. 3c, d), but also possesses some pores with size of ~3 nm spreading over the nanosheets (Fig. 3d). Inset in Fig. 3d is a typical high-resolution TEM image of the as-prepared I-ceria, where the interplanar spacing of the ordered stripes calculated at different orientations is ~0.27 nm, corresponding to (200) lattice plane of ceria.

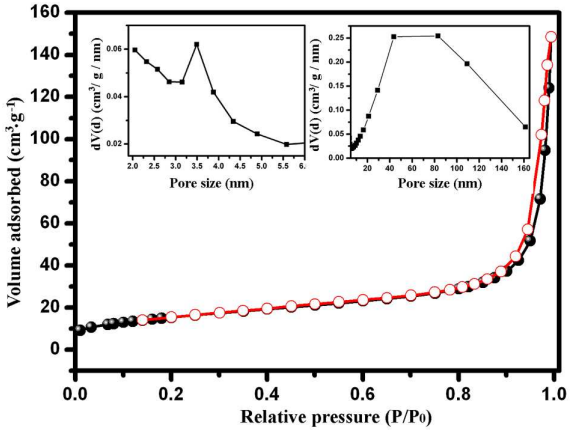

Fig. 4 Nitrogen adsorption-desorption isotherm and the corresponding BJH pore size distribution for the I-ceria sample.

The nitrogen adsorption-desorption isotherm of hierarchically mesoporous I-ceria exhibits the type-H3 hysteresis loop characteristic of mesoporous materials (Fig. 4).[19] The measured BET surface area is around 56 $m^2 \cdot g^{-1}$. The desorption branch almost coincides with the adsorption branch with the presence of a very small hysteresis loop in the range of 0.85-1.0, indicating that the adsorption and desorption processes are mostly reversible. It also indicates that both the mesopores in the nanosheets and the voids between nanosheets are open pores, easily accessible for N_2 molecules. The BJH curves confirm the bimodal pore size distributions possessing small mesopore (~3.5 nm) in the nanosheets and dominant large voids (20-160 nm) spanning from mesopores to macropores within nanosheets, which also agrees well with the SEM/TEM observations.

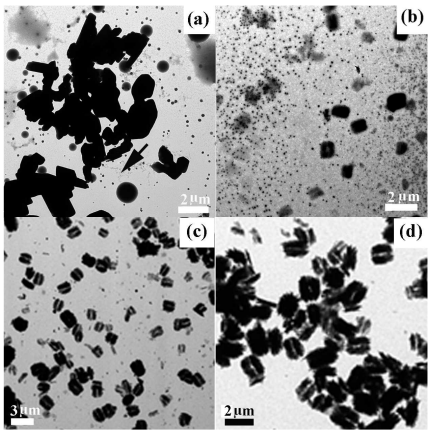

Fig. 5 TEM images of the $Ce_2(SO_4)_3$ precursor prepared at different reaction time: (a) 10 min, (b) 30 min, (c) 1.5 h, and (d) 3 h at 160 °C.

To understand the formation mechanism of such hierarchically hollow $Ce_2(SO_4)_3$ precursor, the time-dependent morphology evolution process was examined thoroughly by TEM. Upon the mixture of H_2SO_4 and $CeCl_3$ in ethanol, a white precipitate quickly produces in the form of irregular particles. When this white slurry was treated at 160 °C for 10 min, a number of sizeable irregular particles were observed mixing with many minuscule connected particles (indicated by an arrow). In addition, it is noticeable that some faceted, well-dispersed particles coexist (Fig. 5a). When the reaction time was extended to reach 30 min, the large irregular particles disappeared and more faceted particles produced, still exhibiting the well monodisperse behavior. However, a few square-like particles and identifiable hollowing within them are clearly observed at this stage (Fig. 5b). After 1.5 h, square-like particles with hollow structure become predominant over faceted particles (Fig. 5c). When the reaction was extended to 3 h, almost all of the particles exhibited the similar square and hollow morphology (Fig. 5d). Based on the above results, it is proposed that the formation of the hierarchically hollow $Ce_2(SO_4)_3$ is a result of the combination of dissolution-recrystallization and assembly processes. When the initial $Ce_2(SO_4)_3$ white slurry was heat-treated, the large particles that were formed at the early stage, dissolved and recrystallized in the form of connected tiny particles. As the reaction time was extended, these connected particles assembled into facet particles, followed by final hierarchically hollow texture in order to reduce the total surface free energy.[21, 22] For the formation of I-ceria, there is a solid-liquid interface reaction between the $Ce_2(SO_4)_3$ and OH^- when the $Ce_2(SO_4)_3$ was mixed with NaOH ethanol solution. The $Ce_2(SO_4)_3$ dissociates Ce^{3+} slowly to combine with OH^- to form $Ce(OH)_3$, which is easily oxidized and converted into ceria on exposure to open atmosphere. The density reduction from $Ce_2(SO_4)_3$ to ceria and the release of water from the $Ce_2(SO_4)_3$ precursor could generate holes, resulting in mesoporous structure in I-ceria. A similar transformation process has been observed for other materials.[33, 34]

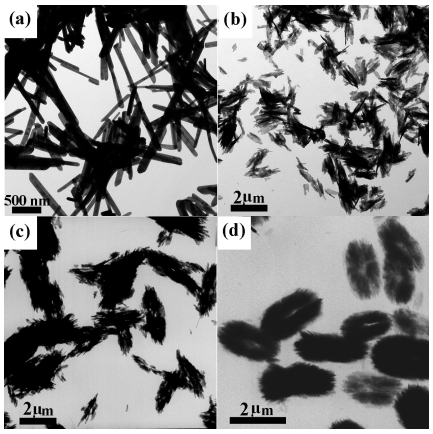

Fig. 6 TEM images of the $Ce_2(SO_4)_3$ precursor prepared at different sulfuric acid concentration: (a) 1 M, (b) 2 M, and (c) 3 M, (d) 4 M at 160 °C for 3 h.

Controlled experiments were carried out to investigate the influence of the sulfuric acid concentration on the morphology of $Ce_2(SO_4)_3$ while other experimental conditions were kept constant. As shown in Fig. 6, the as-prepared $Ce_2(SO_4)_3$ displays rod-like morphology when 1 M of H_2SO_4 (1 ml) is added into $CeCl_3$ ethanol solution (Fig. 6a). With the increase of acid concentration from 2 M to 5 M, various kinds of bunches in the form of rod (Fig. 6b), spindle (Fig. 6c), and rectangle (Fig. 6d), square (Fig. 2, 3) were obtained, respectively. It was reported that hydrated $Ce_2(SO_4)_3$ is easy to form chain structure due to its inherent crystal growth habit.[32] When the volume ratio of ethanol/water increases, the decrease of solvent dielectric constant causes rods' length decrease,[35] while the decrease of the

solubility of $Ce_2(SO_4)_3$ increases the tendency of supersaturation, which also favors the formation of shorter rods.[36] These rods, therefore, self-assemble into hierarchical structures with different aspect ratios.

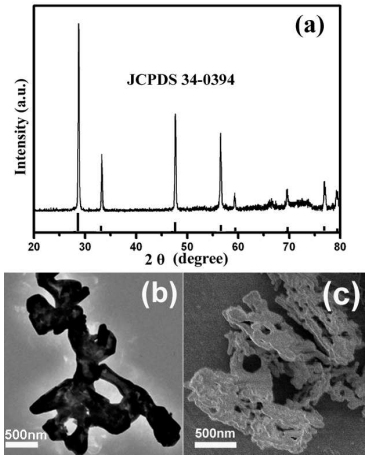

Fig. 7 (a) XRD pattern, (b) TEM and (c) SEM images of the sample prepared by calcination of $Ce_2(SO_4)_3$ precursor at 850 °C for 2 h.

As stated above, it is a general way to achieve metal oxide from the calcination of the desired precursors. When the hierarchically hollow textured $Ce_2(SO_4)_3$ is calcined at high temperature (up to 850 °C for 2 h), it can be transformed into ceria. As shown by the XRD pattern in Fig. 7a, all of the diffraction peaks are well matched with that of the ceria (JCPDS: 34-0394), and the sharp narrow peaks indicate that the C-ceria sample has a good crystallinity. The BET surface area of C-ceria is only 9.3 $m^2 \cdot g^{-1}$, which is much lower than that of I-ceria. In addition, there are no mesopores within C-ceria derived from nitrogen adsorption-desorption isotherm (Fig. S2). The hierarchical structure was severely damaged after calcination; even the square profile of particles was hardly kept (Fig. 7b and c). The calcination treatment has, obviously, a significant impact on keeping hierarchical porous structure intact.

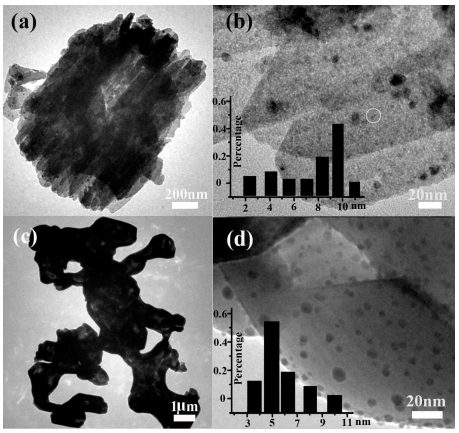

Fig. 8 TEM images of the I-ceria/Au (a, b) and C-ceria/Au (c, d) composites with different magnification. Insets in (b) and (d) display the histograms with the particle size distributions of Au NPs.

Catalytic oxidation of CO to CO_2 is always one of the hottest topics in the catalysis fields due to its important industrial applications, such as car-exhaust emission control, chemical processing, and fuel cell. In addition, it is also an ideal model reaction to further study the mechanism of heterogeneous catalysis.[37-41] Among different types of catalysts, ceria supported Au NP catalyst has been extensively studied towards CO oxidation. Herein, Au NPs were deposited on both C- and I-ceria by deposition-precipitation method. The total Au loading content of the I-ceria/Au was 2.70 wt % and C-ceria/Au was 2.62 wt %, respectively, as determined by ICP-MS. As shown in Fig. 8, it is clear that Au NPs were dispersed on both I- and C-ceria. However, the Au NPs exhibit a wide size distribution in I-ceria/Au sample, where 8~10 nm sized NPs and identifiable ~2 nm sized ones (as denoted by circle in Fig. 8b) coexist. For C-ceria/Au sample, the size of most Au NPs is in the range of 4-7 nm (Fig. 8d). The light-off curves of I-ceria, C-ceria and their corresponding ceria/Au composites, for CO oxidation are presented in Fig. 9a. Obviously, the I-ceria exhibits higher catalytic activity than that of C-ceria for both individual ceria and Au/ceria composites. Specifically, ~69% CO conversion is reached at 300°C for I-ceria, while only ~8% CO conversion at the same temperature for the C-ceria. For ceria/Au nanocomposites, 50% CO conversion is realized at ~54 °C with I-ceria/Au in clear contrast to ~238 °C with C-ceria/Au. Obviously, the addition of Au NPs significantly increased the catalytic activity of both kinds of ceria. To study the durability of the I-ceria/Au catalyst, the sample had been continuously used for 36 h under CO oxidation conditions. As shown in Fig. 9b, CO oxidation of 81% could still be achieved with only ~9% catalytic deactivation in comparsion with initial conversion at 100°C. The Au NPs still remain highly dispersed on I-ceria support and are not obviously agglomerated (inset in Fig. 9b), indicating that the I-ceria/Au catalyst has a good durability.

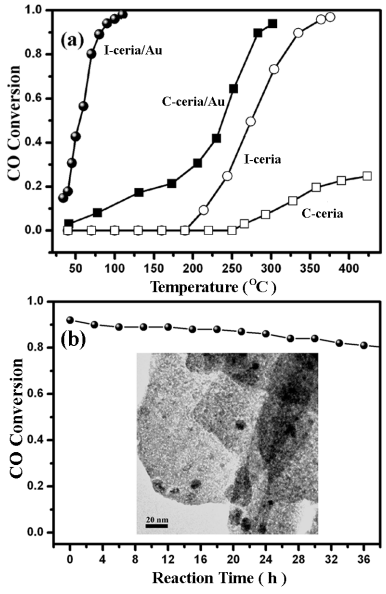

Fig. 9: (a) CO conversion as a function of temperature for I-ceria/Au, C-ceria/Au, I-ceria and C-ceria; (b) Stability of I-ceria/Au catalyst at 100°C for catalytic oxidation under the conditions of (a). Inset in (b) is the TEM image of I-ceria/Au catalyst after 36 h catalytic reaction.

To clarify their difference in catalytic activities, we used XPS to characterize chemical states of Ce, O and Au species on the catalyst surface. All of the presented Ce 3d XPS spectra were similar; there was no appreciable shift in the binding energy from one sample to another (Fig. 10 a). In the O1s XPS spectra, the O1s signal clearly shows two different surface oxygen species. The low binding energy peak (O_α: 529-530 eV) is ascribed to lattice oxygen and the shoulder peak (O_β: 531-532.8 eV) is assigned to defective or adsorptive oxygen species. As shown in the Fig. 10 b and Fig. S3, the O_β peaks in both I-ceria and I-ceria/Au are obviously stronger than those in C-ceria samples. In general, ceria with higher surface area and smaller particle size tends to have more crystal edges and corners, which, in turn, produce higher concentration of surface oxygen species. During the CO oxidation, ceria could supply reactive oxygen in the form of surface adsorptive oxygen species, which is known to be favorable to the improvement of CO catalytic activity.[23] The XPS spectra of Au 4f were also taken on the I-ceria/Au and C-ceria/Au samples. As shown in Fig. 10 c, d, the Au 4f ionization process is characterized by the doublet of the two spin-orbit components, Au $4f_{7/2}$ and Au $4f_{5/2}$, with a splitting of 3.7 eV. The Au presents a main Au $4f_{7/2}$ component at a binding energy of ~84 eV, typical of metallic Au^0, in C-ceria/Au sample. In contrast, in addition to metallic Au^0, broadened shoulders on the high binding energy side can be assigned to the oxidation state of $Au^{\delta+}$ (Fig. 10 c and Fig. S4). The positive role of $Au^{\delta+}$ species in CO oxidation has been widely accepted because they promote CO_2 desorption in the CO oxidation process.[42]

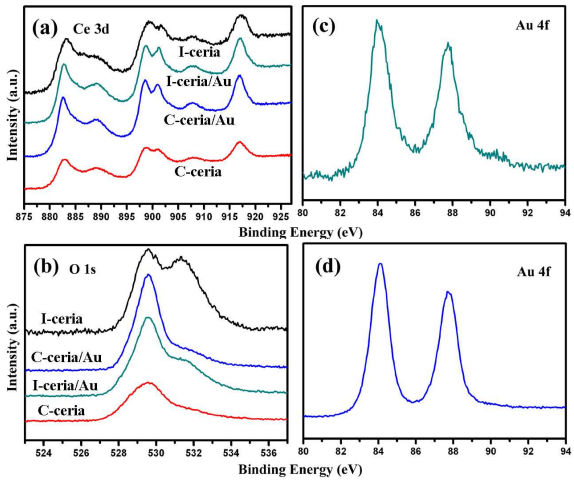

Fig. 10 (a) Ce 3d (b) O 1s XPS spectra of I-ceria/Au, C-ceria/Au, I-ceria and C-ceria; Au 4f spectra of (c) I-ceria/Au and (d) C-ceria/Au.

H_2-TPR was also used to test the reduction behavior of ceria and ceria/Au composites. The H_2-TPR curve for ceria normally consists of two main peaks. One is located at 300-600°C, corresponding to a reduction of surface oxygen species of ceria, which is generally considered as the active oxygen in the low-temperature oxidations. The other one is located at around 800°C, corresponding to a reduction of bulk oxygen species in ceria, which has insignificant contribution in CO oxidation.[25] In Fig. 11, the amount of hydrogen consumed by the surface oxygen species in H_2-TPR process is higher for I-ceria than that for C-ceria, reflecting from broading peak at 300-600 °C in the TPR curve of I-ceria. The incorporation of Au into ceria significantly modifies the TPR profiles. The surface ceria reduction peaks become largely diminished at 300-600 °C, giving rise to new reduction peaks, centered at ~120°C for I-ceria/Au and ~170 °C for C-ceria/Au, respectively. The lower reduction peak of I-ceria/Au, in compared with C-ceria/Au, can be viewed as indications of a stronger interaction between Au NPs and ceria, higher oxygen mobility, and more surface active oxygen, which are advantageous for the CO oxidation.[25, 43]

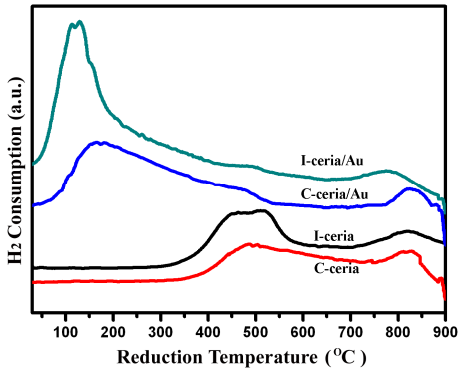

Fig. 11 (a) H_2-TPR profiles of I-ceria/Au, C-ceria/Au, I-ceria and C-ceria.

Conclusions

In summary, we have developed a facile method to construct hierarchical mesoporous ceria via a solid-liquid interfacial reaction between $Ce_2(SO_4)_3$ precursor and NaOH. The key points during the synthesis include (1) utilization of a water-soluble precursor; (2) room temperature and surfactant/polymer-free synthesis; (3) avoidance of a calcination step. After interfacial reaction at room temperature, the I-ceria inherits well the hierarchically hollow structure of $Ce_2(SO_4)_3$ precursor and exhibits mesoporous structure, which enables it to be an ideal support for Au NPs in CO oxidation. In contrast, the C-ceria derived from direct calcination of $Ce_2(SO_4)_3$ precursor displays severe sintering. This work represents a good demonstration of an interfacial reaction-engaged process capable of generating hollow nanostructures from water-soluble precursors. When other suitable water-soluble precursors are chosen, this method is expected to be implemented to the fabrication of other hollow metal oxide materials.

Acknowledgements

This work is supported by the National Natural Science Foundation of China (Grant no. 21173131).

Notes and references

[a] *School of Chemistry and Chemical Engineering, University of Jinan No.336 Nanxinzhuang west road, Jinan (P. R. China) Tel: (86)-531-82769181; E-mail: chm_chengz@ujn.edu.cn*
[b] *School of Chemistry and Chemical Engineering, Shandong University No. 27 Shanda south road, Jinan (P. R. China)*
†Electronic Supplementary Information (ESI) available: TEM image of $Ce_2(SO_4)_3$ precursor under higher magnification, Nitrogen adsorption-desorption isotherm and the corresponding BJH pore size distribution for the C-ceria sample, and the curve-fitting of O1s, Au 4f XPS spectra. See DOI: 10.1039/b000000x/.

1 X. Liu, K. Zhou, L. Wang, B. Wang and Y. Li, *J. Am. Chem. Soc.* 2009, **131**, 3140-3141.
2 B. Liu, Q. Wang, S. Yu, T. Zhao, J. Han, P. Jing, W. Hu, L. Liu, J. Zhang, L.-D. Sun and C.-H. Yan, *Nanoscale* 2013, **5**, 9747-9757.
3 J. Qi, J. Chen, G. Li, S. Li, Y. Gao and Z. Tang, *Energy Environ. Sci.* 2012, **5**, 8937-8941.
4 N. Ta, J. Liu, S.Chenna, P. A. Crozier, Y. Li, A. Chen and W. Shen, *J. Am. Chem. Soc.* 2012, **134**, 20585-20588.
5 C. Sun, H. Li and L.Chen, *Energy Environ. Sci.* 2012, **5**, 8475-8505.
6 H.-X. Mai, L.-D. Sun, Y.-W. Zhang, R. Si, W. Feng, H.-P. Zhang, H.- C. Liu and C.-H. Yan, *J. Phys. Chem. B* 2005, **109**, 24380-24385.
7 Y. Gao, W. Wang, S. Chang and W. Huang, *ChemCatChem.* 2013, **5**, 3610-3620.
8 Q. Wang, W. Jia, B. Liu, W. Zhao, C. Li, J. Zhang and G. Xu, *Chem. Asia. J.* 2012, **7**, 2258-2267.
9 X. W. Lou, L. A. Archer and Z. Yang, *Adv. Mater.* 2008, **20**, 3987-4019.
10 X. Wang, D. Liu, S. Song and H. Zhang, *Chem. Eur. J.* 2013, **19**, 8082-8086.
11 J. Wang, N. Yang, H. Tang, Z. Dong, Q. Jin, M. Yang, D. Kisailus, H. Zhao, Z. Tang and D. Wang, *Angew. Chem. Int. Ed*. 2013, **52**, 6417-6420.
12 C. Sun, H. Li and L. Chen, *Energy Environ. Sci*. 2012, **5**, 8475-8505.
13 A. Trovarelli (ed), Catalysis by Ceria and Related Materials, *Catalytic Science Series* 2002, **2**, 217-243.
14 C. Wen, Y. Zhu, Y. Ye, S. Zhang, F. Cheng, Y. Liu, P. Wang and F. Tao, *ACS Nano* 2012, **6**, 9305-9313.
15 L. Almar, T. Andreu, A. Morata, M. Torrell, L. Yedra, S. Estradé, F. Peiró and A. Tarancón, *J. Mater. Chem. A* 2014, **2**, 3134-3141.
16 Q. Yuan, H.-H. Duan, L.-L. Li, Z.-X. Li, W.-T. Duan, L.-S. Zhang, W.-G. Song and C.-H. Yan, *Adv. Mater.* 2010, **22**, 1475-1478.
17 P. Xu, R. Yu, H. Ren, L. Zong, J. Chen and X. Xing, *Chem. Sci.* 2014, **5**, 4221-4226.
18 J. Qi, K. Zhao, G. Li, Y. Gao, H. Zhao, R. Yu and Z. Tang, *Nanoscale* 2014, **6**, 4072-4077.
19 N. Zhang and Y.-J. Xu, *Chem. Mater.* 2013, **25**, 1979-1988.
20 L.-Shu Zhong, J.-S. Hu, A.-M. Cao, Q. Liu, W.-G. Song and L.-J. Wan, *Chem. Mater.* 2007, **19**, 1648-1655.
21 C. Sun, J. Sun, G. Xiao, H. Zhang, X. Qiu, H. Li and L. Chen, *J. Phys. Chem. B* 2006, **110**, 13445-13452.
22 J. Chen, S. Zhong, Q. Liu, Y. Wang, S. Wang, R. Xu, L. Luo and S. Wang, *Powder Technol.* 2010, **197**, 136-139.
23 W. Liu, L. Feng, C. Zhang, H. Yang, J. Guo, X. Liu, X. Zhang and Y. Yang, *J. Mater. Chem. A* 2013, **1**, 6942-6948.
24 S. Song, H. Wang, A. Song, S. Dong and J. Hao, *Chem. Eur. J.* 2014, **20**, 9063-9072.
25 H. Li, G. Lu, Q. Dai, Y. Wang, Y. Guo and Y. Guo, *ACS Appl. Mater. Interfaces* 2010, **2**, 838-846.
26 G. Chen, S. Sun, X. Sun, W. Fan and T. You, *Inorg. Chem.* 2009, **48**, 1334-1338.
27 C. Yan and D. Xue, *J. Phys. Chem. B* 2006, **110**, 7102-7106.
28 J. Fei, Y. Cui, X. Yan, W. Qi, Y. Yang, K. Wang, Q. He and J. Li, *Adv. Mater.* 2008, **20**, 452-456.
29 G. Chen, F. Rosei and D. Ma, *Adv. Funct. Mater.* 2012, **22**, 3914-3920.
30 G. Chen, C. Xu, X. Song, W. Zhao, Y. Ding and S. Sun, *Inorg. Chem.* 2008, **47**, 723-728.
31 G. Chen, C. Xu, X. Song, S. Xu, Y. Ding and S. Sun, *Cryst. Growth Des.* 2008, **8**, 4449-4453.
32 B. M. Casari and V. Langer, *Z. Anorg. Allg. Chem.* 2007, **633**, 1074-1081.
33 Z. Jing and J. Zhan, *Adv. Mater.* 2008, **20**, 4547-4551.
34 J. C. Yu, A. Xu, L. Zhang, R. Song and L. Wu, *J. Phys. Chem. B* 2004, **108**, 64-70.
35 G. Chen, S. Sun, W. Zhao, S. Xu and T. You, *J. Phys. Chem. C* 2008, **112**, 20217-20221.
36 S.-F. Chen, S.-H. Yu, J. Jiang, F. Li and Y. Liu, *Chem. Mater.* 2006, **18**, 115-122.
37 G. Li and Z. Tang, *Nanoscale* 2014, **6**, 3995-4011.
38 H.-P. Zhou, Y.-W. Zhang, H.-X. Mai, X. Sun, Q. Liu, W.-G. Song and C.-H. Yan, *Chem. Eur. J.* 2008, **14**, 3380-3390.
39 J. Fan, X. Jiang, H. Min, D. Li, X. Ran, L. Zou, Y. Sun, W. Li, J. Yang, W. Teng, G. Li and D. Zhao, *J. Mater. Chem. A* 2014, **2**, 10654-10661.
40 K. Yoon, Y. Yang, P. Lu, D. Wan, H.-C. Peng, K. S. Masias, P. T. Fanson, C. T. Campbell and Y. Xia, *Angew. Chem. Int. Ed.* 2012, **51**, 9543-9546.
41 J. Qin, J. Lu, M. Cao and C. Hu, *Nanoscale* 2010, **2**, 2739-2743.
42 J. Zhang, G. Chen, M. Chaker, F. Rosei and D. Ma, *Appl. Catal. B* 2013, **132-133**, 107-115.
43 R. Si and M. Flytzani-Stephanopoulos, *Angew. Chem. Int. Ed*. 2008, **47**, 2884-2887.

Graphical Abstract

Hierarchically porous ceria was successfully synthesized via an interfacial reaction between water-soluble $Ce_2(SO_4)_3$ precursor and NaOH in ethanol. Neither additional surfactant molecules nor calcination was employed during the preparation process.